J Membrane Biol (2015) 248:241–255
DOI 10.1007/s00232-014-9764-7

Conformational Dynamics of *Shaker*-Type Kv1.1 Ion Channel in Open, Closed, and Two Mutated States

Rajabrata Bhuyan · Alpana Seal

Received: 3 November 2014 / Accepted: 21 November 2014 / Published online: 2 December 2014

Abstract The dynamic properties of *shaker*-type Kv1.1 ion channel in its open, closed, & two mutated (E325D & V408A) states embedded in DPPC membrane have been investigated using all-atom force field-based MD simulation. Here, we represent the detailed channel stability, gating environment of charge-carrying residues, salt bridge interaction among the voltage-sensing domains (VSDs), movement of S4 helix, and ion conduction of pore. At positive potential, the S4 helix undergoes lateral fluctuations in accordance with their gating motions found in every model. During transition from closed to active state conformation, charged residues of S4 move "up" across the membrane with an average tilt angle difference of 24°, which is more consistent with the paddle model of channel gating. The E325D mutation at C-terminal end of S4–S5 helical linker leads the channel to a rapid activated state by pushing the gating charge residues upward beside the VSDs resulting in more prominent tilt of S4. Similarly in V408A mutant model, disruption of hydrophobic gate at S6 C-terminal end takes place, which causes the violation of channel-active conformation by bringing the C-terminal end of S4 to its corresponding resting state. The ion permeation is observed only in open-state conformation.

Keywords Voltage-gated potassium channel · Mutation · Episodic ataxia · E325D · V408A

R. Bhuyan
Department of Biochemistry & Biophysics, BIF Centre, University of Kalyani, Kalyani 741235, West Bengal, India
e-mail: rajabrata001@gmail.com

A. Seal (✉)
Department of Biochemistry & Biophysics, University of Kalyani, Kalyani 741235, West Bengal, India
e-mail: aseal@klyuniv.ac.in

Introduction

Voltage-gated potassium (Kv) channels are the most common type of membrane proteins that respond to the transmembrane potential across the membrane and allow the passage of K^+ ions by altering their conformation (Hille 1992, 2001). Hence, they are very essential for balancing the action potentials in the excitable cells, mostly in neurons, lymphocytes, heart muscle, and kidney cells (Gutman et al. 2005; Mert 2006). Kv1.1 is a member of the *Shaker* subfamily of delayed rectifier voltage-gated potassium channels encoded by *KCNA1* gene in human. All the members of this Kv1.x (*Shaker*) family typically show single-channel permeation characteristics that conduct the permeation of K^+ ion at the rate of $\approx 10^7$ ions s^{-1} channel^{-1} (Heginbotham & MacKinnon 1993; Grissmer et al. 1994; Conforti & Millhorn 1997; Conforti et al. 2000). Other than its usual K^+ transportation, it also has a vital role in controlling the action potential duration at the cortical pyramidal neuronal axon by inactivating all the Kv1 channels (Debanne et al. 2011; Bucher & Goaillard 2011). Mutations in Kv1.1 cause hyperexcitation of mammalian axon which is further developed into several neurological disorders such as episodic ataxia with or without myokymia and epilepsy (Browne et al. 1994; Zuberi et al. 1999). Till date, a total of 17 mutations have been identified in Kv1.1 channel, and among them, E325D & V408A are considered to be very critical for the malfunctioning of channel properties (Adelman et al. 1995).

In the ensuing few decades after the Hodgkin–Huxley experiment (Hodgkin & Huxley 1990), scientists have shown their tremendous interest to understand the principles behind Kv channels for their ion conduction. All the members of this *Shaker*-type voltage-gated potassium channels are believed to share the same mechanism for

action potential regulation; hence, they required to have a common core structure. However, the sequence comparison of the selectivity filter and the transmembrane helices show highly conserved amino acid compositions among all the members of this type of ion channels (Shealy et al. 2003). The architecture of Kv1 channels reveals that these are the modular structure with identical tetramers forming a central pore comprising six transmembrane helical segments (S1–S6) in each unit. The first four helices (S1–S4) form an anti-parallel helical unit at the periphery of the channel which is known as voltage-sensing domain (VSD) and the last two helices, S5 & S6, form the ion selective pore. S4 helix contains positively charged amino acids in its every third position, which sense the transmembrane potential across the bilayer and executes the channel opening/closing (Sigworth 1994; Seoh et al. 1996; Aggarwal & MacKinnon 1996; Bezanilla 2000). The VDSs are connected to the pore domain by an amphipathic α-helix (S4–S5 linker) which remains parallel to the membrane. The hydrophobic amino acids of this linker are exposed to lipid, whereas the hydrophilic residues, located in the side facing water, make it stable (Long et al. 2005). The channel maintains the resting state at membrane hyperpolarization, and during the depolarization, the driving force acts on the S4 helix, which pulls the S4–S5 linker toward S6, resulting in the movements of VSDs in each subunit. This mechanism accomplishes the whole protein to undergo a heavy structural change for the transition between active & closed states of conformation (Bezanilla et al. 1994; Zagotta et al. 1994; Smith-Maxwell et al. 1998; Jensen et al. 2010, 2012).

Many crystal structures of eukaryotic *shaker*-type potassium channel of family 2 (Kv1.2) in open-state conformation has been solved and deposited in RCSB (Long et al. 2005, 2007; Tao et al. 2010; Chen et al. 2010; Banerjee et al. 2013). To understand their voltage-gating mechanisms at atomic level, the knowledge of both active and resting conformational states is necessary. But there is not a single atomic resolution structure of a Kv in the resting state till date. In this regard, computational techniques have helped to interpret the results of various wet-lab experiments into structural insights to provide closed-state conformation. Although the Kv1.1 shares same family of voltage-gated potassium channel with Kv1.2, its independent structural study has not progressed so far. Similarly, E325D and V408A mutations in Kv1.1 are believed to induce an unstable open-state conformation, resulting in ~10-fold increase in activation/deactivation rates (D'Adamo et al. 1999), but the structural mechanism is still unknown. In this present study, our focus is on the conformational dynamics of Kv1.1 channel in both wild-type open and closed states as well as in its two mutated states (E325D & V408A) in DPPC lipid bilayer. Using MD simulation, we addressed their stability, analyzed the movement & interactions of the charged residues, behavior of selectivity filter and ion conduction through the pore. We also have provided some useful information and clues about gating mechanism of Kv1.1 ion channel and malfunctioning activities of mutant.

Materials and Methods

Structural Models of Kv1.1 Channels

The structures of human Kv1.1 were carefully constructed in active, resting, and mutated states by homology-based protein structure prediction algorithms using MODELLER (Eswar et al. 2008) of DISCOVERY STUDIO 2.5 program. Atomic models of Kv1.2 in the open and closed states proposed by Pathak et al. accomplished by the Rosetta-Membrane structure prediction program were taken as the template (Pathak et al. 2007). All the generated models were refined via loop optimization, and on the basis of DOPE score, final models were chosen. The transmembrane regions of all the subunits were achieved via energy minimization by smart minimizer of DISCOVERY STUDIO. The backbone RMS deviations of all the energy-minimized tetrameric open, closed, E325D, & V408A mutant models were found to be 1.51, 1.921, 1.587, & 4.692 Å, respectively, from their corresponding templates. Amino acid sequences were downloaded from UNIPROT protein database, and all types of sequence analyses were done using NCBI BLAST (Johnson et al. 2008) and CLUSTALX (Larkin et al. 2007) sequence analysis program. The stereochemistry and structural conformations of those generated models were validated by various servers available at Structural Analysis and Verification Server (SAVES) (http://nihserver.mbi.ucla.edu/SAVES/).

System Preparation and MD Simulation

All the tetrameric models of Kv1.1 were protonated at the physiological pH 7.0 and embedded into pre-equilibrated dipalmitoylphosphatidylcholine (DPPC) bilayer by aligning the protein's axis of symmetry with the bilayer normal using the transformation matrix predicted by TMDET server (Tusnady et al. 2005). The box dimension in z-direction was decreased from cytoplasmic to transmembrane unit of all protein in the simulation system. All the simulations were performed using GROMACS 4.6.3 packages employing gromos54a7 force field (Hess et al. 2008). The DPPC coordinates were taken from D. Peter Tieleman's website, and Berger's lipid parameters (Berger et al. 1997) combined with gromos force field were applied to describe each system. SPC/E (extended simple-point

charge model) water model (Berendsen et al. 1987) was used to solvate each system explicitly, and a salt concentration of 0.10 M KCl was maintained to achieve the entire system electrically neutral. All the unwanted water molecules remaining at the membrane and pore regions were removed from the system manually. Energy minimizations were performed using steepest descents integrator in order to enable protein–lipid packing. Details of all the four simulation boxes are described in Table 1. Three K^+ ions and two water molecules were placed in the pore at alternative positions of each model, where they are suggested to be the most energetically favorable (Aqvist and Luzhkov 2000). A 100 ps NVT equilibration was performed at 323 K by restraining all of the backbone protein atoms to reorient water around exposed proteins and lipid head groups, as well as to reorient lipids around the protein. Then the systems were allowed for 3 ns restrained MD run (NPT), during which only non-hydrogen protein atoms were restrained to enable the water and lipid bilayer packing properly around the protein. For the temperature and pressure coupling during equilibration, the velocity rescale thermostat (Bussi et al. 2007) and semi-isotropic Parrinello–Rahman barostat (Parrinello & Rahman 1981) was applied, respectively. During the final 50 ns production run, all the restraints were removed and the temperatures of the protein, lipid, and solvent (waters and ions) were separately coupled using the Nosé–Hoover thermostat (Nosé 1984) at 323 K, with a coupling time constant of (τT) of 0.8 ps. Similarly, all the system pressures were semi-isotropically coupled by Parrinello–Rahman barostat at 1 bar, via a coupling constant of $\tau P = 2$ ps and compressibility at 4.5×10^{-5} bar^{-1}. Periodic boundary conditions were considered in all the three planes, and the electrostatic interactions were calculated according to the Particle Mesh Ewald (PME) algorithm (Darden et al. 1993). Cutoffs of 12 Å were used for both the Coulombic and van der Waals interactions with a Fourier grid spacing distance of 1.6 Å. All bond lengths were constrained using the linear constraint solver (LINCS) algorithm (Hess et al. 1997). At default positive potential gradient, all the simulations were performed.

All the works were performed in a 32-node Lenovo D30 workstation. Adaptive Poisson–Boltzmann Solver (APBS) (Baker et al. 2001) was used to calculate interaction energy profile of various ions with the pore. Secondary structure plots were carried out by DSSP (Kabsch & Sander 1983), and pore radius was computed using CAVER 3.0 program (Chovancova et al. 2012). The rest of the analyses were performed by Gromacs analysis suite, VMD (Humphrey et al. 1996), and DS 2.5. MS excel program was used to prepare the charts.

Results and Discussion

Models of Kv1.1 in Open, Close, and Mutant States

The Kv1.1 channel shares ~80 % sequence identity with Kv1.2 protein which has full-length crystal structure in its open state. Sequence alignment of human Kv1.1& Kv1.2 reveals that both the proteins must possess very similar type of secondary structure pattern in their corresponding transmembrane helices, and the sequence variability is observed only at the extracellular/intracellular interconnecting loops between these helices. These transmembrane linkers are characterized with highly flexible loops. Studies suggest that the linkers, which are exposed to external solutions, provide a glycosylation site, necessary for the channel activities (Zhu et al. 2003; Tu and Deutsch 2010). In addition to S2–S3 and S3–S4 linkers, the segments at S1–S2 loop are a bit more extended, comprising 39 amino acids in Kv1.2 and 34 in Kv1.1 (Fig. 1).

About 37 % of the available Kv1.2 crystal structure was incomplete due to the high dynamics and/or static disordering. In that case, the activated/open and resting/closed conformations proposed by Pathak et al. (2007) were taken as template to generate the 3D structure of Kv1.1 channel in open, closed, and mutated states using homology-based comparative modeling. Their proposed open model complements the missing information of the X-ray structure with the *de novo* modeled inter-helical VSD loops. Using voltage-clamp fluorometry and theoretical knowledge behind voltage-dependant protein motions, they have derived the closed-state conformation. The voltage sensor S4 helix comprised six gating-charge-carrying residues including five arginines at positions 292, 295, 298, 301, &

Table 1 System composition of simulation boxes

Conformation	No. of lipids	No. of water molecules	No. of K^+	No. of Cl^-	Total no. of atoms	Box size (nm^3)
Open	499	55,149	293	265	207,123	14.99282 × 15.05146 × 13.02354
Closed	498	54,595	295	267	205,415	15.05146 × 15.05146 × 13.02354
E325D	499	55,213	295	267	207,315	15.05146 × 15.05146 × 13.02354
V408A	500	54,854	293	265	206,280	14.99282 × 15.05146 × 13.02354

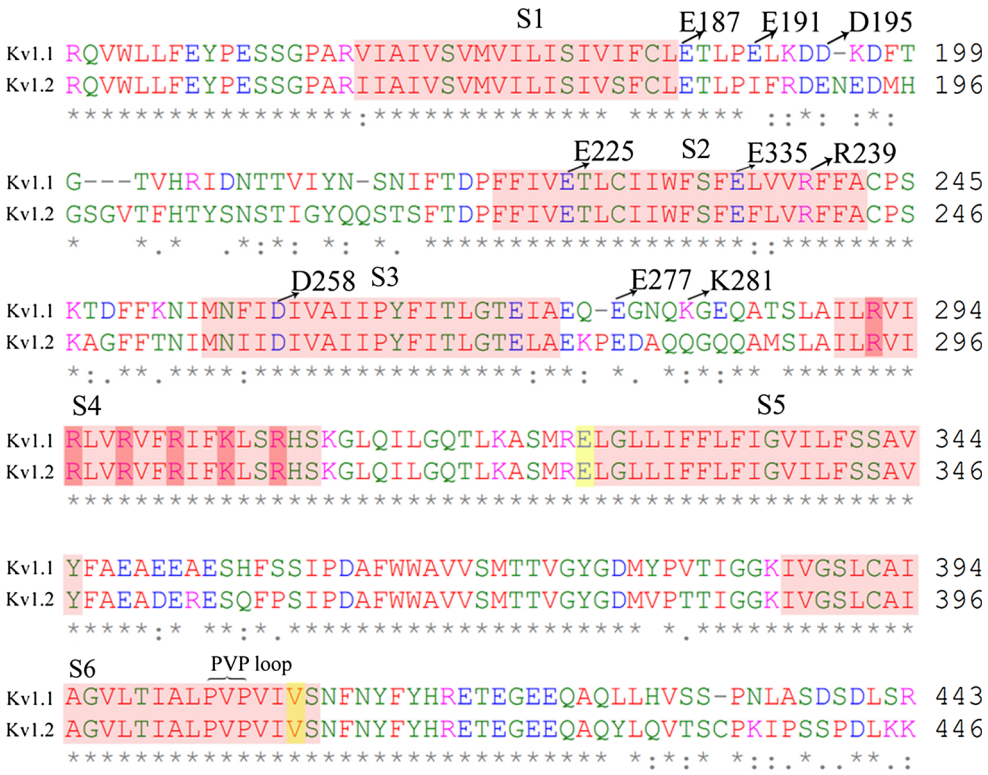

Fig. 1 Sequence alignment of human Kv1.1 & Kv1.2. *Highlighted portions* are transmembrane helices and S4 charged residues. The E325D & V408A mutation points are marked in *yellow* (Color figure online)

307 and one lysine at 304 in Kv1.1, termed as R1, R2, R3, R4, R6, and K5, respectively (Fig. 2). Initial interaction of these charged residues within the same subunit in all the four models were described as follows. In open state, the S4 top residues R1 and R2 were positioned near the membrane–water interface. R3 at position 298 was surrounded by two glutamic acid residues (E187 or E0 & E191) at the end of S1 helix forming salt bridge (Fig. 2e). Similarly, the deeper R4, K5, and R6 were, respectively, paired with Glu225 (E1) of S2, Asp258 of S3, and Glu235 (E2) of S2, which is in good accordance with both experimental & previous simulation studies (Tiwari-Woodruff et al. 1997, 2000; Papazian et al. 1995; Treptow & Tarek 2006; Jogini & Roux 2007; Bjelkmar et al. 2009). The early model of closed state proposed by Pathak et al. (2007) was more uncertain, though it was broadly consistent with experimental constraints. Latter, this model has been refined by Khalili-Araghi et al. (2010) using all-atom MD simulations and highly reliable Rosetta algorithms. Moreover, the stabilized closed conformations obtained from engineered cross-link and metal bridge studies were also more consistent with established experimental findings (Campos et al. 2007; Henrion et al. 2012). In our closed model, the R1 was very close to E1 following both the theoretical and experimental consequences (Tombola et al. 2005). The initial conformation of E325D showed very close resemblance with the open model. But in V408A, S4 was found fairly close to S1 & S2 helices, and four (R3, R4, K5, and R6) out of six charged residues of S4 participate in salt bridge interaction with these helices (Fig. 2). The physical and functional dynamics of these four models are well achieved through all-atom computer simulation.

Conformational Stability of All Four Models

Overall stabilities of all the four models are monitored through the Cα RMSD, root-mean-square fluctuations (RMSF), and secondary structure assessment (DSSP) studies (Fig. 3). The Cα RMSD provides a picture of the global drift from all the starting conformations in open, close as well as in two mutated states, as shown in Fig. 3a. In open state, the RMSD of the transmembrane regions increases rapidly up to the level of ∼5 Å during the first 30 ns of simulation and maintains its stability almost at 4.5 Å during rest of the time scale. This rapid deviation may occur as a result of the relaxation of protein in lipid bilayer. However, the voltage sensor S4 helix deviates within 2.5–3.0 Å, which can be considered as a principal contributor of whole channel RMSD. The central pore-forming residues (TVGYGD, 372-377) shared by all the four chains remain almost rigid from the rest parts of protein. Unlike the open-state conformation, all the transmembrane helices in closed-state model are little bit more excited. This overall deviation is affected mainly by the motion of VSDs where, all the charged residues of S4 helix move to their respective native positions inside the

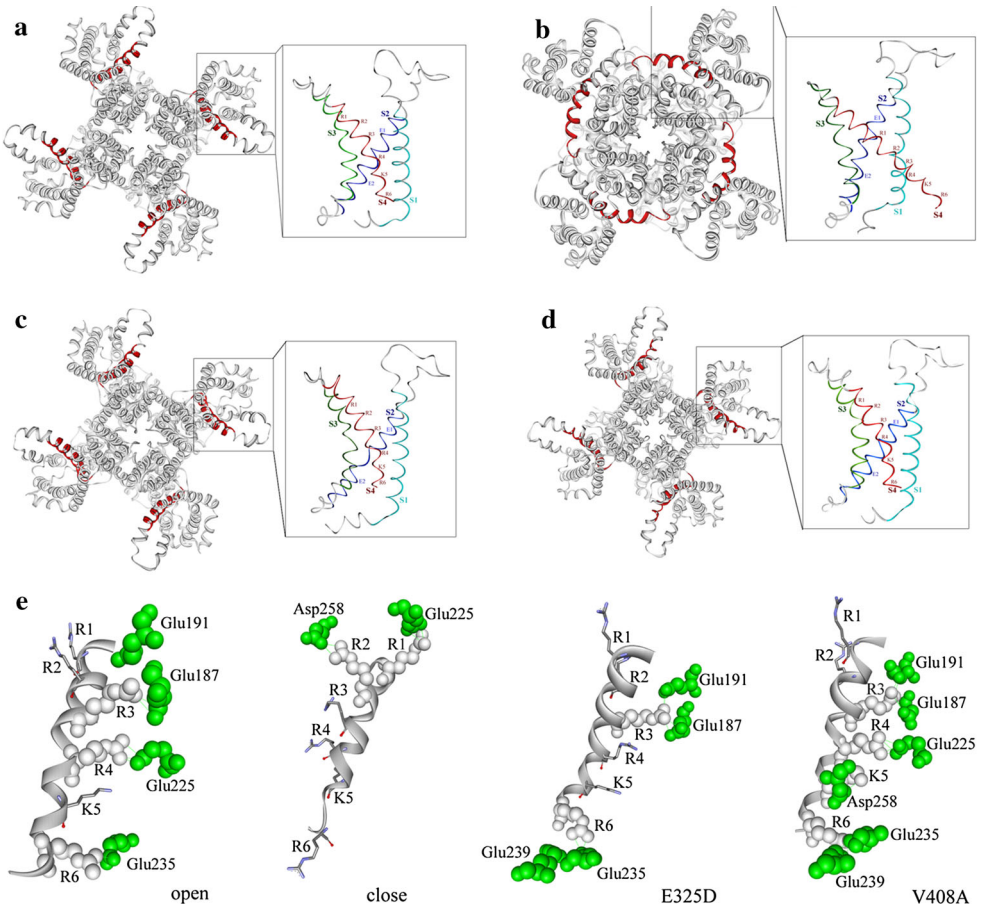

Fig. 2 Initial models Kv1.1 channels showing voltage-sensing domains distinctly, **a** open, **b** close, **c** E325D & **d** V408A mutation model. **e** Neighboring amino acids of the S4 gating residues in *open*, *close*, *E325D*, & *V408A* mutation model (Color figure online)

membrane to attain its resting-state conformation. Similarly, the RMS deviation of ion-selective pore in closed model is comparatively high with open state (Fig. 3a).

In case of E325D, the transmembrane Cα RMSD takes more time for stabilization and reaches to a proper equilibrium state at 40 ns of simulation. However, the V408A mutated model does not seem to be stabilized till the end. The S4 helix and pore region of E325D & V408 models reach the equilibrium state at 2.5 & 2.0 Å and 2.5 & 1.5 Å of RMSD, respectively, from their initial conformations.

The Cα root-mean-square fluctuations (RMSFs) in each model taking average of all the identical chains as a function of their residue number show that the transmembrane helices of VSDs remain stable in all systems (Fig. 3b). The drifts in the RMSF profile mainly correspond to the inter-helical loops. The initial prominent peaks (at *N*-terminal region) in the graph describe the flexible intracellular parts in all models. In open-state conformation, the helical link between the cytoplasmic and transmembrane segment (just before the S1) is highly mobile and turned into two separate helices, and one of them forms a bend-like conformation (Fig. 3b, c). The same pattern is also observed in two mutated models, which are possibly due to the movement of transmembrane helices during the protein–lipid packing. But it is almost steady in closed conformation throughout the simulation time.

The S1–S2 linker region is a large loop resides above the membrane and fluctuates most remarkably in all the models. This linker has always been an interesting issue, because the N-terminal gating residues of S4 interact with it. In open state, a short α helix is formed within this loop which separates away from the rest of the protein and remains more stable in comparison with other models (Figs. 3c, 4). It is also believed that the extended region of S1–S2 linker firmly binds with the outer pore helix during the opening of Kv channels, which is necessary for its proper function (Lee et al. 2009). So the formation of this short α helix in S1–S2 linker and its separation from the protein may have some effect on voltage-dependent opening. In closed model, this loop is a bit more extended and fluctuates highly, but remains intact within the VSDs. Previous simulations on Kv1.2 suggest that the S1–S2 linker in active state is more mobile than inactive/closed conformation and supposed to have mostly a random coil, lacking helical structure (Bjelkmar et al. 2009; Khalili-

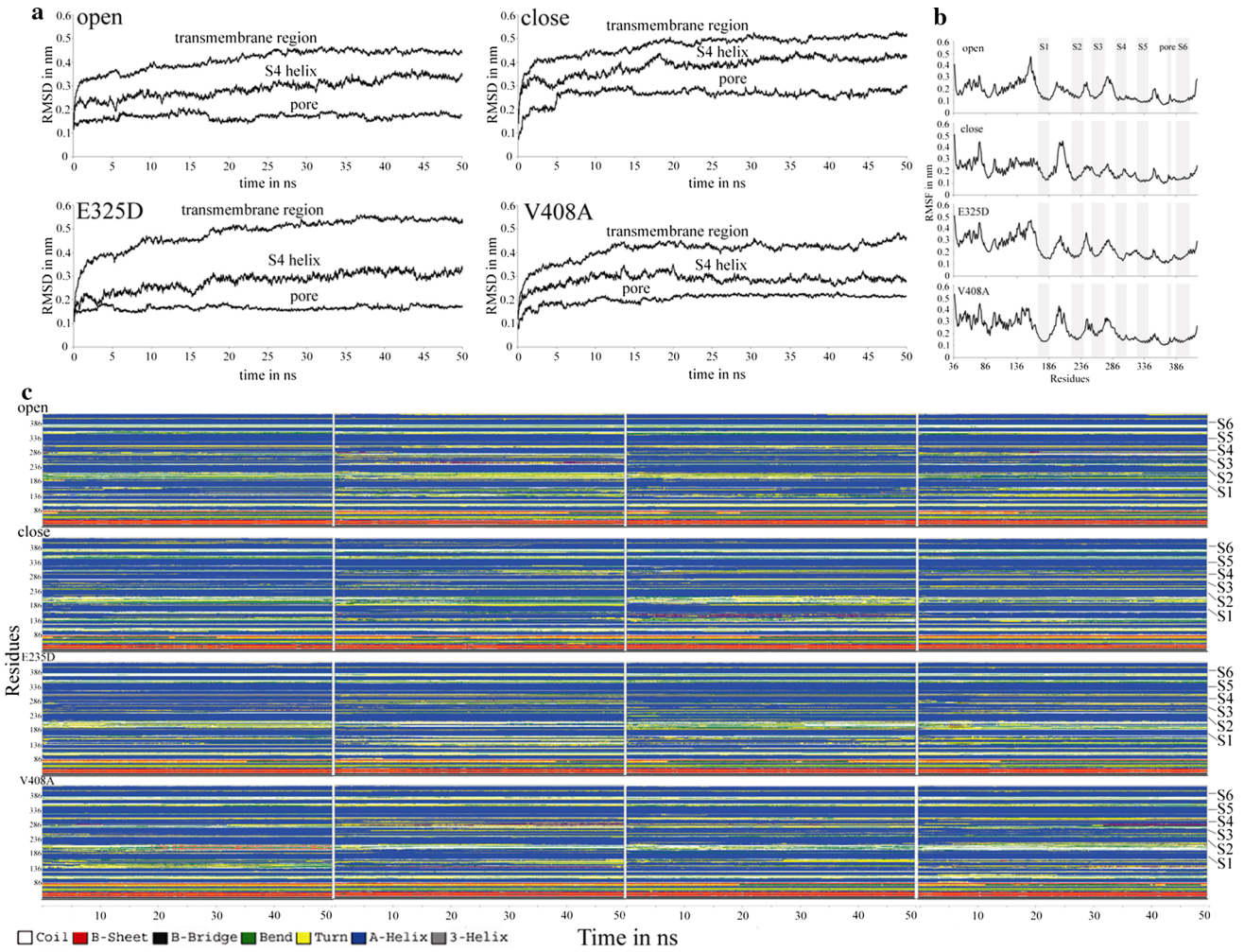

Fig. 3 **a** RMSD of Cα residues in transmembrane segments, voltage sensor, and pore of all the four models with respect to time. **b** RMS fluctuation as a function of residue number. The transmembrane regions are marked by *shadows*. **c** DSSP profile as a function of simulation time. The identical subunits of each model are listed *horizontally* (Color figure online)

Araghi et al. 2010). On the other hand, the active-state crystal structure reported by Long et al. (2007) confirms a short helical segment in this S1–S2 linker. In addition, no constant secondary structure in this particular region is concluded from our simulation of both the mutant models. But in E325D mutant, this linker is interestingly forwarded slightly toward the S5 helix interacting with S5–S6 segment via numerous H-bonds (Fig. 4). Incidentally, the stability of S1 and S2 helices of any model is not affected by the high mobility of the S1–S2 loop connecting these two transmembrane parts. All the helical segments are comparatively more stable in open-state model than the others. The difference grows visible only in S3 & S4 helices where they intend to interact with the lipid head groups. Meanwhile in closed state, they reside almost near to the core of membrane as well as the pore-forming helices. Interestingly, the S3 & S4 in the mutant cases fluctuate appreciably with an average difference of 0.05 and 0.02 nm, respectively, from the open state.

According to the crystal structure of active-state Kv1.2 channel, the intracellular end of the S4 helix adopts a 3_{10} conformation (Long et al. 2007; Clayton et al. 2008). This idea of 3_{10} helical propensity at 7–10 lower-end residues in S4 helix is further validated by Villalba-Galea et al. (2008). They have shown that both the active- and resting-state conformation possess a 3_{10} helical conformation in S4 C-terminal end. But a slow transition from 3_{10} to α helix takes place during the channel in active relaxed state. In our study, 3_{10} helical transformation is seen in every subunit of E325D mutated model and two subunits of open model, which may be aided by the correct electric field as a component of voltage sensing by the charged residues of S4. RMSF plot of selectivity filter or the pore domain of all the models show notable stability compared to the voltage

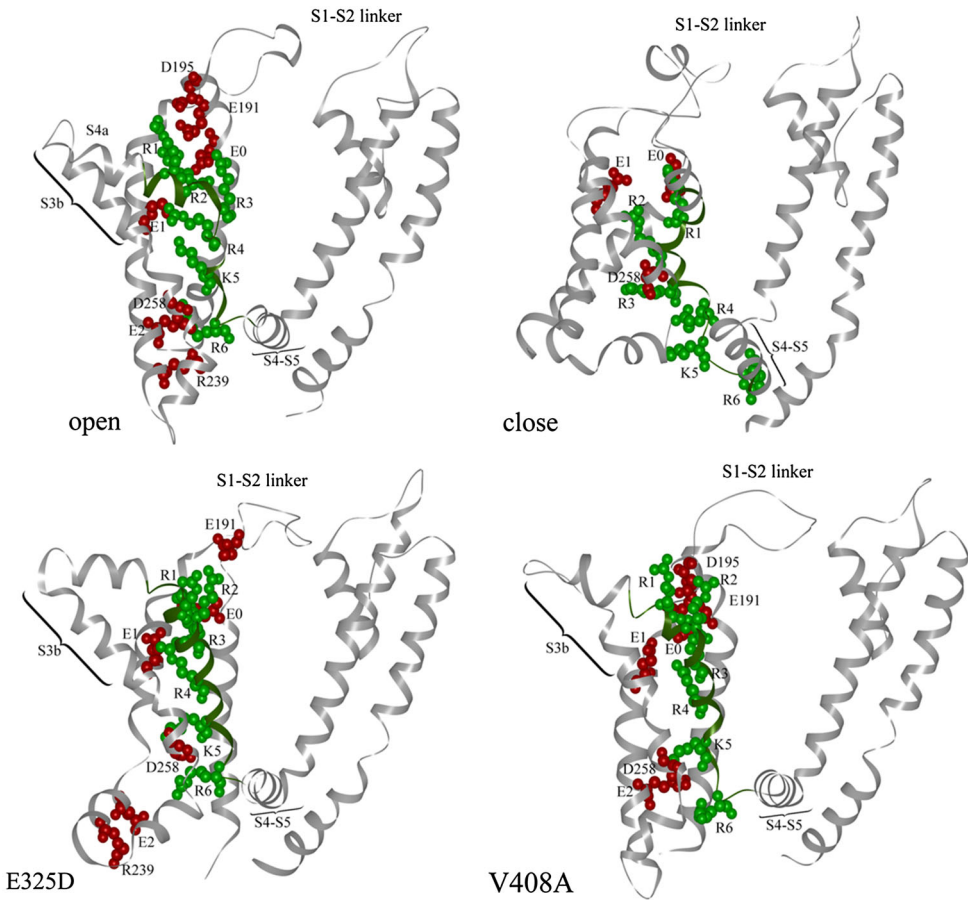

Fig. 4 VSDs conformation of all the four models. S4 key residues are *colored in green*, and their corresponding interacting amino acids are mentioned in *red* (Color figure online)

sensor S4 helix which is agreed by the RMSD graphs also. The solvent-exposed loop S4-S5 linker, which transfers the driving force during the channel activation, shows more excited in closed & E325D model, but maintains remarkable steady helical feature in open and V408A mutant. Since this type of ion channel takes several milliseconds for the transition between open and closed conformations and it's a matter of too long time span for atomistic MD simulation, we only concentrated on the comparison of the conformational dynamics in these four states of Kv1.1 ion channel at their equilibrium in this study.

Interaction of Voltage Sensor-Charged Residues

The change in transmembrane potential generates the gating current with the help of gating-charge-carrying residues in VSDs. The different subunits of all the four models lost their symmetry due to the displacement of those charged residues just after few picoseconds of simulation. Especially, S4 is the most affected one where arginine or lysine is present in every third position along the helix. It is believed that the salt bridge formation between the conserved basic side chains of S4 and some specific acidic residues along S1, S2, & S3 helices are vital for their folding, stability, and function of the VSDs (Papazian et al. 1995; Seoh et al. 1996; Tiwari-Woodruff et al. 1997). We observed several patterns of hydrogen bonds and salt bridge formations of these charged residues in all the four models which correspond to their conformational changes and stability during the depolarized state.

The first two arginine residues (R1 & R2) of S4 are found to be positioned near the membrane layer and participate in forming numerous stable salt bridges and hydrogen bonds with DPPC in open, E325D, & V408A mutated models. But in closed conformation, R1 & R2 are surrounded by S1, S2, & S3 helices only. Unlike the Kv1.2, initial salt bridge of R1 with E1 (GLU225 of S2) is sacrificed just after few ns of simulation with a new persistent salt bridge with E0 (GLU187). This phenomenon is quite possible, because there is another glutamic acid (GLU191) present at the end of S1 helix in Kv1.1, which is absent in Kv1.2. This negatively charged residue patch (GLU187, GLU191, and ASP195) can attract the R1 more toward them in Kv1.1 in comparison with Kv1.2. R2 & R3 of all models except the closed state interact with the negatively charged amino acids like E0 or E191 or D195 at the

C-terminal end of S1 helix via salt bridges. In two chains of V408A mutant, a fresh salt bridge between R3- E1 is noticed and this interaction is already found in a single chain of closed model where, R2 & R3 are conventionally supposed to interact with D258 of S3. R4 & K5 are solely located in the protein environment in every chain of all the models except the closed one. In closed-state conformation, R4, K5, & R6 are faced to the membrane surface and found interacting with the lipid by numerous stable salt bridges and H-bonds. But in two chains of open model, E1 forms stable salt bridge with K5 and in another two, D258 takes its place. Similarly, in all the subunits of E325D mutated model, K5 interacts with E1 & D258, whereas E2 & D258 form stable salt bridges with K5 in V408A mutated state. On the other hand, R6 of open model is exposed next to the S2 & S3 helix as well as the lipid bilayer and interacts with E2 or R239 and D258 via two stable salt bridges. While in E325D mutant, both the E2 & R239 stay free from any of those charged residues and R6 forms salt bridge pair with D258. No interaction between R6 & D258 is observed in any of the subunits in case of V408A mutated model and R6 remains free from the rest (Fig. 4).

Some specific movements of those key residues of S4 segment in all the four models are monitored via some particular salt bridge interaction. The E0-R3 pair was conserved in open and both the mutant models at the beginning. But during the simulation, R4 is shifted toward E0 and provides consistent salt bridge in both the mutant models. E1 of S2 interacts with both the R4 & K5 of open & E325D mutant model, while the K5 of V408A is exposed deep into the lower leaflet of membrane bilayer having no contact with E1. The E2 of S2 helix participates in electrostatic interaction with R6 of open and at the beginning in mutant models, which gets disappeared just after few ns, and K5 forms stable salt bridge with E1 only in V408A model. In two subunits of open and all units of E325D model, the side chain of R6 at the intracellular end of S4 provides a stable and long-lasting interaction with D258. But in case of V408A mutant, K5 takes the place of R6 in all the subunits. From these observations, we are able to conclude that the whole S4 helix in E325D and only the extracellular upper part of S4 in V408A model move apparently in upward direction in accordance with the open conformation. Whereas, the S4 lower-end residues of V408A shift down to the membrane core. However, these findings are significantly correlated with the result of individual drift by these charged residues. Another peculiar stable salt bridge between E277-K281 is observed in E325D mutant and three subunits of open model. This interaction works as connector between S3 and S4 helices. Distance of the same salt bridge in all the subunits of V408A mutant increases with time and is completely absent in closed model. Nevertheless, this is an exceptional property of Kv1.1 as lysine is replaced by a glutamine at position 281 in Kv1.2.

Drift of the S4 Segment

The relative movement of S4 helix inside VSD core is already described to couple the voltage sensing with channel gating. In order to characterize the gating motions of S4, we traced the vertical movements (the z-axis parallel to the membrane normal) of these charged residues lining along the helix. In each model, all the charged residues of S4 move from their initial position to an energetically favorable environment where they can be well hydrated and paired with acidic side chains and/or lipid head groups. The vertical displacements of these residues (taking average of four chains) along the z-axis are shown in Fig. 5.

In open-state conformation, the overall shift of all these key residues is observed in a same manner. An early upward displacement of S4 takes place around 5 Å in the protein core and then stabilizes after 20 ns of simulation with some extent of downward movement (Fig. 5a). The average drift of S4 charged residues are recorded with upward displacement of $\sim$1.5 Å from its initial conformation. Starting from the beginning, S4 in closed model moves toward the intracellular region and provides several stable electrostatic interaction and H-bonds within the lipid bilayer (Fig. 5b). A remarkable upward movement of all the key residues is observed in E325D mutated model (Figs. 5c, 6). After 10 ns of simulation, the S4 turns toward the S1-S3 helices and no charged residue is found at the S4 extracellular end extensively exposed to the hydrocarbon chains of the lipids (Fig. 5c). But a striking feature is observed in case of V408A mutation, where the tendency of individual drift for each of the charged residues takes place. The vertical locations of R1 & R2 shift deep into the protein core and stabilize after 20 ns of simulation (Fig. 5d). On the other hand, R6 is not directly stabilized by any acidic residues of S2 or S3 and moves toward the lipid membrane to interact with them. The other residues R3, R4, & K5 maintain almost their original position throughout the simulation. Initial differences in the vertical movements of R1, R2, R3, R4, K5, and R6 in closed-state conformation with reference to the open model were 0.38, 0.73, 0.83, 0.48, −0.03, and −0.30 nm, respectively, and reach to 0.41, 0.74, 0.81, 0.62, 0.27, and −0.24 at equilibrium after 35 ns of simulation (Fig. 5e). That implies during transition between closed and open states of conformation, the C-terminal end of S4 may have major impact on gating charge transfer.

The average tilt angle of S4 helix along the bilayer plane was calculated from the trajectories of each simulation model. In our simulation, the S4 segments of open and

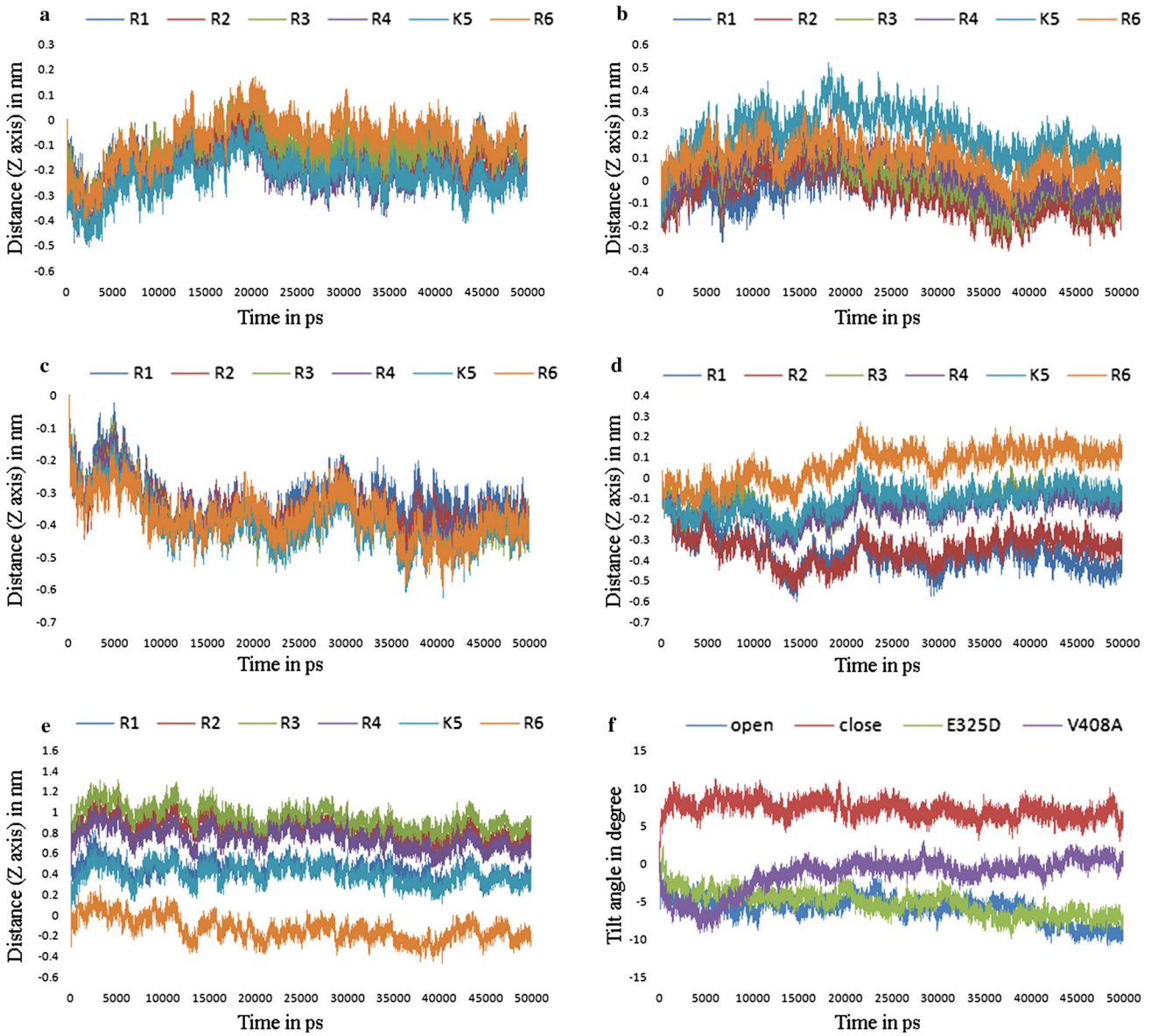

Fig. 5 Movement of the Cα atoms of charged residues in S4 helix from their initial position given in z-direction; **a** in open, **b** closed, **c** E325D, & **d** V408A model, **e** closed model with reference to open, **f** change in tilt angle of S4 in all the four models (Color figure online)

E235D model tilt more toward the protein core from their initial position, while in closed state, it is found to be stabilized in opposite direction. It is because of the polarization effect of the channel where, the intracellular end of S4 goes across the membrane producing an opposite tilt to the open activated conformation (Zagotta et al. 1994; Long et al. 2005). Consequently, in V408A mutated model, the tilt angle change takes place in a similar pattern with the open model for 5 ns of simulation and then shifts in the reverse direction around 10° with a close resemblance to the resting state model (Fig. 5f). The initial tilt angle difference between the closed and open states of conformation was 11° which increased to a balanced value of ∼24° at 40 ns of simulation after a big fluctuation.

Water Crevices Inside VSDs

It is believed that the water molecules fill the empty crevice at the center of VSDs by both sides of membrane, and all positive-charged residues of S4 get hydrated, which influences the transmembrane potential. This is actively valuable in some extent while it helps to move the positively charged side chains of S4 to the aqueous crevice and get interacted with the negatively charged residue along S2 and

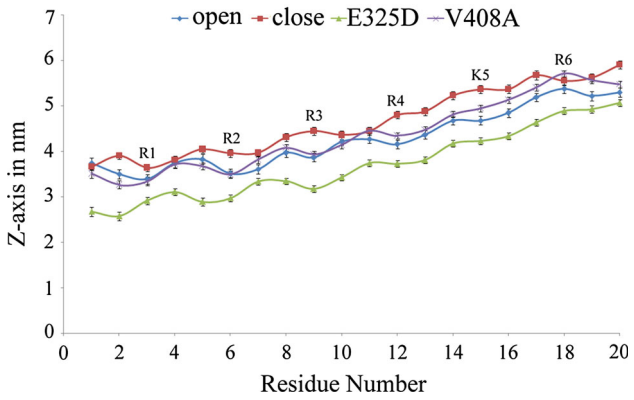

Fig. 6 Average amino acids positions in S4 helix along z-axis at equilibrium of all models (Color figure online)

S3. This aqueous crevice feature has been inferred in many previous experiments and simulation studies (Starace and Bezanilla 2001; Jogini and Roux 2007; Bjelkmar et al. 2009; Tombola et al. 2007). In our open-state conformation, comparatively more amount of water penetrates to the intracellular S4 surface than the extracellular part. This trend is followed in two other mutated models also. However, in E325D, due to the exponential tilt of S3 & S4 extracellular region, a narrow water crevice is formed at external side and the top charged residues R1, R2, R3, & R4 are less hydrated. The widest crevices are observed in closed-state conformation where almost all the charged residues are exposed to water and both the ends of crevice are separated by R2. These water crevices serve as dielectric medium, which cause the VSDs to drop high transmembrane potential in contrast to the surroundings.

Channel Gating and Role of Mutation

The perspective of gating mechanism of Kv-type ion channel is established by several experimental and computational studies. The most consistent scenario of voltage-dependant activation of Kv channels is the function of major conformational changes in their S4 helix. Usually at rest, all the charged residues of S4 remain in the so-called "down state" interacting with the intracellular bilayer leaflet and negatively charged residues of other VSDs at extracellular water crevices. During activation, S4 segment moves outward through the focused transmembrane field and connects the lipids at both ends (Bezanilla et al. 1994; Khalili-Araghi et al. 2010; Jensen et al. 2012). From our simulation, we achieved the equilibration states of both open and closed model of Kv1.1 which is consistent with the numerous previous simulations studies. The salt bridge network and vertical drift of key residues of S4 in all models depict that the S4 helix moves from intracellular to extracellular binding site with a distance of 6–8 Å during the transition between closed and open states of conformation. This is very similar with the studies by Pathak et al. (2007). We also observed that the intracellular end of S4 in V408A moves down toward the membrane core, which is against the usual configuration of active Kv channel. While the S4 of E325D mutated model adopts the "up" conformation during equilibrium (Fig. 6).

Besides the upward movement of S4 helix, the tilt of S3b-S4a segment along the membrane axis also supports "paddle model" of voltage-gated activation in Kv channel (Chanda et al. 2005). S3b-S4a segment is a "helix-turn-helix" motif, also known as the "VS paddle", formed by the C-terminal S3 and the N-terminal portion of the S4, packed tightly together and anchor the channel with external membrane leaflet (Jiang et al. 2003; Ruta et al. 2005; Swartz 2004, 2008). However, the bend of this VS paddle is believed to be regulated by the S2–S3 linker and crystallographic structure of Kv1.2 has revealed the possibilities of many local distortion in this linker as well as in both the terminus of S3 (Long et al. 2007). Hence, these conformational flexibilities tend the S3b–S4a ''paddle'' to move relatively toward the rest of VSDs resulting in the channel opening during depolarization. The driving force required for this transition is controlled by the S4–S5 linker helix, which separates the VSDs from pore domain. The E325D mutation is located at the C-terminal end of this S4–S5 linker helix and differs from the wild type by a single-side chain carbonyl group. In our simulations, we observed a high degree of conformational flexibility at both the S4a and S3b part of open and E325D mutated model (Figs. 3, 5). However, extremely affected positional displacement of S4 charged residue as well as the paddle movement is observed in E325D channel. Several mutational and toxic binding studies of Kv channels justify that S4–S5 linker in open activated conformation must be extended to the N-terminal regions of S5 interacting with S6, which play the crucial role in controlling the electrostatic interaction between phosphate lipid head groups and the outer S4, responsible for the channel opening or closing (Soler-Llavina et al. 2006; Milescu et al. 2009). Hence, it is feasible for an aspartic acid to form more salt bridge interactions when glutamic acid is absent in its place and enable the S4-S5 linker to remain intact toward S5. This mechanism necessarily enhances the paddle movement by pushing the S4 helix to remainder of the VSDs in E325D mutated model, which may imply a strong gating effect causing the malfunction of Kv1.1 channel.

The major gating conformational changes in Kv channels are also guided by two hydrophobic gates located at the intracellular end of S6 helix (Jensen et al. 2010). Ile400 is placed at upper gate over the mostly conserved Pro-Val-Pro (PVP motif) residues constituting the lower one. The whole hydrophobic pocket is stabilized by many other

hydrophobic residues lying at S6 lower end including V408, which resides just at one helical turn intracellular to the lower gating pocket. Recently, Jensen et al. (2012) has described the mechanistic details about hydrophobic gating in Kv channels. At depolarized potential when the S4 helix moves upward, the first proline (P403) of PVP motif and Leu329 of S5 interchange their side chains, developing a kink at lower end of S6, which allows the ion-selective pore to get hydrated. Simultaneously, the upper gate goes activated and enables the ion conduction. However, during the channel at resting state, Leu329 & Pro403 transiently move away from each other and Pro403 gets close to Ile400, resulting in a bent at upper gate. Previous studies have reported that substitution of V408 by an alanine enhances the current decay in Kv1.1 channel by inducing an activated-not-open conformation (Jensen et al. 2010). Perhaps, it happens due to disruption of S6 hydrophobic core by insertion of a less-hydrophobic alanine in the place of valine. However, this destabilization effect is clearly visualized in V408A mutant model from our simulation. We observed the increasing distance between P403 and L329 in V408A as well the PVP motif gets closed with the upper hydrophobic gate (Table 2). Hence, rather than forming a lower gate kink in S6, a tiny bend is formed at Ile400 (Fig. 7). This illustration is also reflected in the downward movement of intracellular end of S4 helix, where it attempts to adopt its relaxed state (Figs. 5, 6). The driving force of the open activation gate can no longer transfer from the S4 to the pore, and the VS paddle starts to move back ensuing a reverse tilt compared to active conformation (Figs. 4, 5).

Again due to the bend of S6 in V408A mutation, an arginine at the lower end gets more exposed to the linker helix connecting the transmembrane and cytoplasmic unit of channel, which contains highly conserved acidic residues such as D133, E134, E139, E140, & E141 (Fig. 7). The attraction of these negatively charged amino acids by the arginine causes the total disruption of this linker as well as the whole cytoplasmic unit to get separated from each other. This may also be a practical reason for the destabilization of Kv1.1 channel with V408A mutation.

Table 2 Distances between the hydrophobic residues in all models with standard deviations in Å

Models	L329-P403	I400-P403
Open	6.74 ± 0.35	7.08 ± 0.33
Closed	7.40 ± 0.70	5.75 ± 0.30
E325D	6.81 ± 0.36	6.93 ± 0.36
V408A	7.27 ± 0.33	6.64 ± 0.21

The Ion-Selective Pore

The ion-selective pore of this family of ion channel is located in the middle of transmembrane region, surrounded by four VSDs from all the monomeric units. This segment is composed by both polar and non-polar residues, forming a stretch of signature sequence "TVGYGD", contributed by all the four chains (Zhou and MacKinnon 2004). During positive potential gradient, the VSDs go for large conformational changes enabling the opening of the central ion conduction pore and grant the outward flow of K^+ ion from cell. However, it behaves as the most stable transmembrane unit in comparison with the others. To verify the competence of ion selectivity in Kv1.1 channel, we calculated the interaction energy profile in its open-state conformation along central pore axis taking several ions like Na^+, K^+, Rb^+, and Cs^+. The graph illustrates that the arrangement of all these ions near the pore is very much favorable except only the Na^+. When the ions were positioned at the intracellular end, the interaction energy was absolutely zero and it increased up to some extent when they move upside and suddenly start to reduce rapidly near the pore-lining region, between 20 and 50 Å along z-axis (Fig. 8). Doyle et al. (1998) have given lucid evidences about the doable passage of Rb^+ and Cs^+ ions through this type of voltage-gated potassium channel. Our findings also support the same. The relatively small Na^+ ion in the channel pore is not favorable for Kv channels, and hence it proves the reliability and the selectivity conformation of pore residues of our models.

Ion Conduction

Side chain carboxyl groups of the highly conserved selectivity pore residues provide four and one extended binding sites (S0-S4) for K^+ ions (Zhou and MacKinnon 2004). Under physiological ion concentration, the selectivity filter is occupied by two or three K^+ ions along with two water molecules separating their positions. There are two specific configurations by which the K^+ ion and water molecule can be hold by the pore; either the K^+ ions reside at sites 1 and 3, separated by a water molecule at site 2 or at sites 2 and 4 with a water molecule at site 3 (Bernèche and Roux 2000; Zhou and MacKinnon 2003). Initially, we placed three K^+ ions at sites 0, 2, & 4 with water at sites 1 & 3 in all the four simulation models, but ion passage is detected only in open model.

No external force was provided to any of K^+, and all the simulations were performed in positive ion concentration gradient. The trajectories of three K^+ show that the ion placed at S0 site, which is very close to the outer most part of the pore toward the extracellular region, left its position just after few ns of simulation. The S2 site ion was stable in

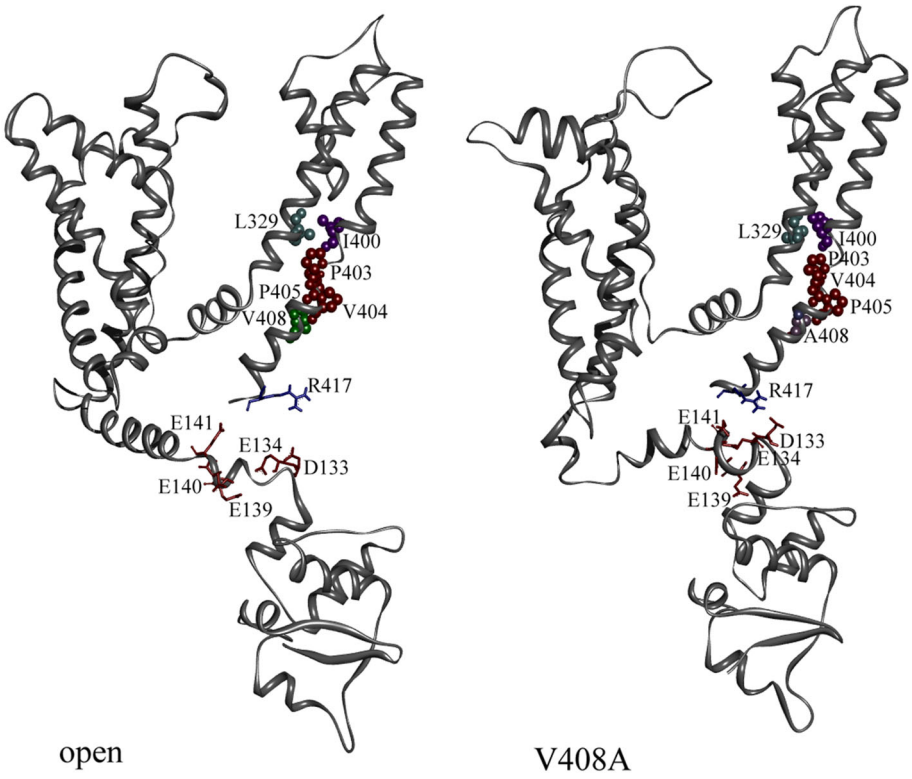

Fig. 7 Monomeric structure of Kv1.1 wild-type open and V408A mutant model at equilibrium (Color figure online)

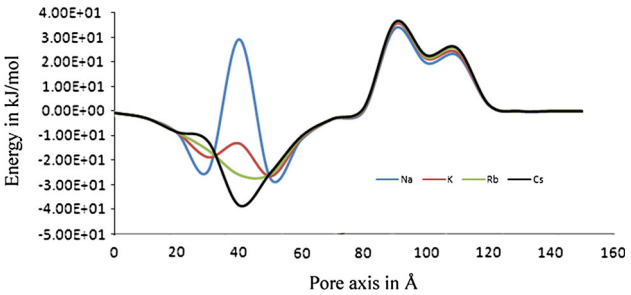

Fig. 8 Interaction energy profile of ions in the central pore axis of open channel (Color figure online)

its position for a very short period and pushed toward S1 within 6 ns of simulation and finally came out of the pore. During equilibrium, the initially positioned K^+ at site 4 moved to site 3 and was steady with S3 site throughout the time scale (Fig. 9). Meanwhile, another potassium ion entered the pore from the intracellular solution and helped to stabilize the S4 site for a long period. The conformational changes of ion-selective pores of all the four models are given below (Table 3).

The average solvent-accessible surface area (SASA) derived from the MD trajectories possessed by the pore residues of open model was 2,126 $Å^2$, which was found a bit lesser than the closed model. It suggests that the side chains of pore residues in closed models are more exposed to the solvents and this data are in unison with the pore radius calculated from the MD snapshots of 50 ns of simulation trajectory. The average pore radius of the closed model is only 1.28 Å, the smallest one in comparison with others. Similarly, the average SASA values found in case of mutated E325D & V408A models are 1,911 & 2,020 $Å^2$, respectively, a consequence to their increased pore size (Table 3). The gating mechanism does not depend directly upon the pore conformation which is one of the most stable

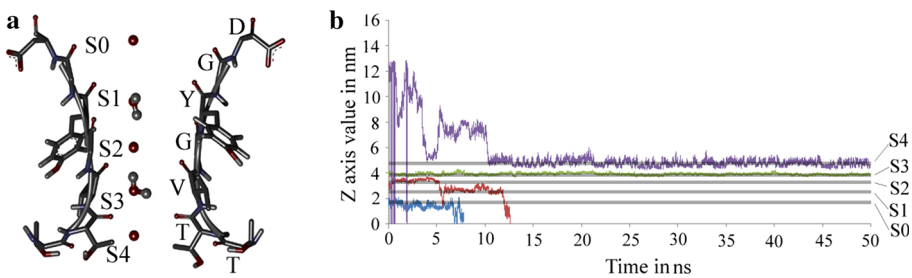

Fig. 9 **a** Ion-selective pore of Kv1.2. **b** Trajectories of K^+ ions in z-axis projected in the pore symmetry of open-state model ion channel. *Separate colors* are used for individual ion (Color figure online)

Table 3 Solvent-accessible surface area of pore region and pore bottleneck radius of pore residues among all the four models

	Open	Close	E325D	V408A
Total SASA in Å^2	2,126 ± 62	2,273 ± 61	1,911 ± 53	2,020 ± 120
Hydrophobic surface area in Å^2	987 ± 43	1,120 ± 38	930 ± 36	945 ± 49
Hydrophilic surface area in Å^2	1,139 ± 36	1,153 ± 42	981 ± 41	1,075 ± 79
Pore radius in Å	1.55 ± 0.34	1.280 ± 0.26	1.74 ± 0.37	1.68 ± 0.37

segments of these types of ion channels. However, this information provides a general glimpse about the selectivity filter of our four models.

Conclusions

In summary, our study reports on the biophysical behavior of *shaker*-type Kv1.1 ion channel in open, closed, and two open mutated states embedded in DPPC bilayer. The structural flexibility of all models was the consequence of their corresponding VSD motions in lipid bilayer. From our comparative analysis of RMSD, RMSF, and DSSP plots, we observed that the residues in pore-lining regions were more stable than the other part of protein and the S4–S5 linker, who serves as transferring the gating charge to pore domain, was comparatively more excited in both the closed and E325D mutants. Similarly, a large structural change occurred in the S1–S2 linker of the channel in resting and V404A states. The depolarization effect was felt in open and E325D mutated models where the intracellular end of S4 turns into a 3_{10} helical transformation.

Electrostatic interaction of charged residues of S4 helix revealed their positional affinities toward membrane or protein core. In open & E325D conformations, these key residues of S4 were found to be mostly interacting with the negatively charged amino acid of S2 & S3 helices and get attached to bilayer by both ends via H-bonds and salt bridges. Meanwhile, in closed model, the intracellular end of voltage sensor pushed to a bit down toward membrane layer and contributed interactions with DPPC. The similar downward movement of intracellular S4 was ensured in V408A mutated model. The conformational flexibility of S3b–S4a ''paddle'' in open & E325D mutant models indicate that, positively charged S4 helix responded to membrane depolarization by its N-terminal S4a segment and moved relative to the rest of the VS domain resulting an intense change in S4 tilt. In the meantime, S4 in V408A moved back to its resting conformation with a reverse tilt.

Ultimately, we have tried to discuss some structural aspects for the channel malfunction in both E325D & V408A mutant models. Our results suggest that the E325D mutation at C-terminal end of S4-S5 helical linker influenced the channel activation by pushing S4 toward the rest of VSDs, which in turn enhanced the "S3b-S4a paddle" movement. Likewise, the disruption of hydrophobic gate at S6 C-terminal end was concluded in V408A mutant model causing the activation gate to close at depolarized potentials. Another distinguished feature of V408A mutation was the bend of S6 more to the cytoplasmic unit. The interaction of R417 with negatively charged residues of that particular cytoplasmic linker induced the destabilization of whole cytoplasmic unit, producing an active-not-open conformation. These findings with implications may be helpful for future strategies to understand the role of mutations in autosomal dominant disorder, episodic ataxia. Obviously, more real experimental and computational work will be needed to further elucidate the nature of both voltage-driven conformational changes as well as the structural significance of mutants in this type of ion channels.

Acknowledgments The authors are thankful to Mr. Suman Kumar Nandy for his valuable suggestions and for reading the manuscript carefully. The whole study was supported by Grants from BTIS net programme of DBT, Ministry of Science & Technology, Government of India, New Delhi and DST purse programme.

References

Adelman JP, Bond CT, Pessia M, Maylie J (1995) Episodic ataxia results from voltage-dependent potassium channels with altered functions. Neuron 15:1449–1454. doi:10.1016/0896-6273(95)90022-5

Aggarwal SK, MacKinnon R (1996) Contribution of the S4 segment to gating charge in the *Shaker* K^+ channel. Neuron 16:1169–1177. doi:10.1016/S0896-6273(00)80143-9

Aqvist J, Luzhkov V (2000) Ion permeation mechanism of the potassium channel. Nature 404:881–884. doi:10.1038/35009114

Baker NA, Sept D, Joseph S, Holst MJ, McCammon JA (2001) Electrostatics of nanosystems: application to microtubules and the ribosome. Proc Natl Acad Sci USA 98:10037–10041. doi:10.1073/pnas.181342398

Banerjee A, Lee A, Campbell E, Mackinnon R (2013) Structure of a pore-blocking toxin in complex with a eukaryotic voltage-dependent K^+ channel. Elife 2:e00594. doi:10.7554/eLife.00594

Berendsen HJC, Grigera JR, Straatsma TP (1987) The missing term in effective pair potentials. J Phys Chem 91:6269–6271. doi:10.1021/j100308a038

Berger O, Edholm O, Jähnig F (1997) Molecular dynamics simulations of a fluid bilayer of dipalmitoylphosphatidylcholine at full hydration, constant pressure, and constant temperature. Biophys J 72:2002–2013. doi:10.1016/S0006-3495(97)78845-3

Bernèche S, Roux B (2000) Molecular dynamics of the KcsA K^+ channel in a bilayer membrane. Biophys J 78:2900–2917. doi:10.1016/S0006-3495(00)76831-7

Bezanilla F (2000) The voltage sensor in voltage-dependent ion channels. Physiol Rev 80:555–592

Bezanilla F, Perozo E, Stefani E (1994) Gating of *Shaker* K^+ channels: II. The components of gating currents and a model of channel activation. Biophys J 66:1011–1021. doi:10.1016/S0006-3495(94)80882-3

Bjelkmar P, Niemelä PS, Vattulainen I, Lindahl E (2009) Conformational changes and slow dynamics through microsecond polarized atomistic molecular simulation of an integral Kv1.2 ion channel. PLoS Comput Biol 5:e1000289. doi:10.1371/journal.pcbi.1000289

Browne DL, Gancher ST, Nutt JG, Brunt ER, Smith EA, Kramer P, Litt M (1994) Episodic ataxia/myokymia syndrome is associated with point mutations in the human potassium channel gene, KCNA1. Nat Genet 8:136–140. doi:10.1038/ng1094-136

Bucher D, Goaillard JM (2011) Beyond faithful conduction: short-term dynamics, neuromodulation, and long-term regulation of spike propagation in the axon. Prog Neurobiol 94:307–346. doi:10.1016/j.pneurobio.2011.06.001

Bussi G, Donadio D, Parrinello M (2007) Canonical sampling through velocity rescaling. J Chem Phys 126:014101. doi:10.1063/1.2408420

Campos FV, Chanda B, Roux B, Bezanilla F (2007) Two atomic constraints unambiguously position the S4 segment relative to S1 and S2 segments in the closed state of *Shaker* K channel. Proc Natl Acad Sci USA 104:7904–7909. doi:10.1073/pnas.0702638104

Chanda B, Asamoah OK, Blunck R, Roux B, Bezanilla F (2005) Gating charge displacement in voltage-gated ion channels involves limited transmembrane movement. Nature 436:852–856. doi:10.1038/nature03888

Chen X, Wang Q, Ni F, Ma J (2010) Structure of the full-length *Shaker* potassium channel Kv1.2 by normal-mode-based X-ray crystallographic refinement. Proc Natl Acad Sci USA 107:11352–11357. doi:10.1073/pnas.1000142107

Chovancova E et al (2012) CAVER 3.0: a tool for the analysis of transport pathways in dynamic protein structures. PLoS Comput Biol 8:e1002708. doi:10.1371/journal.pcbi.1002708

Clayton GM, Altieri S, Heginbotham L, Unger VM, Morais-Cabral JH (2008) Structure of the transmembrane regions of a bacterial cyclic nucleotide-regulated channel. Proc Natl Acad Sci USA 105:1511–1515. doi:10.1073/pnas.0711533105

Conforti L, Millhorn DE (1997) Selective inhibition of a slow-inactivating voltage-dependent K^+ channel in rat PC12 cells by hypoxia. J Physiol 502(Pt 2):293–305

Conforti L, Bodi I, Nisbet JW, Millhorn DE (2000) O_2-sensitive K^+ channels: role of the Kv1.2 α-subunit in mediating the hypoxic response. J Physiol 524(Pt 3):783–793. doi:10.1111/j.1469-7793.2000.00783.x

D'Adamo MC, Imbrici P, Sponcichetti F, Pessia M (1999) Mutations in the KCNA1 gene associated with episodic ataxia type-1 syndrome impair heteromeric voltage-gated K^+ channel function. FASEB J 13:1335–1345. doi:10.1096/fj.1530-6860

Darden T, York D, Pedersen L (1993) Particle mesh Ewald: an $N\cdot\log(N)$ method for Ewald sums in large systems. J Chem Phys 98:10089–10092. doi:10.1063/1.464397

Debanne D, Campanac E, Bialowas A, Carlier E, Alcaraz G (2011) Axon physiology. Physiol Rev 91:555–602. doi:10.1152/physrev.00048.2009

Doyle DA et al (1998) The structure of the potassium channel: molecular basis of K^+ conduction and selectivity. Science 280:69–77. doi:10.1126/science.280.5360.69

Eswar N, Eramian D, Webb B, Shen MY, Sali A (2008) Protein structure modeling with MODELLER. Methods Mol Biol 426:145–159. doi:10.1007/978-1-60327-058-8_8

Grissmer S et al (1994) Pharmacological characterization of five cloned voltage-gated K^+ channels, types Kv1.1, 1.2, 1.3, 1.5, and 3.1, stably expressed in mammalian cell lines. Mol Pharmacol 45:1227–1234

Gutman GA et al (2005) International Union of Pharmacology. LIII. Nomenclature and molecular relationships of voltage-gated potassium channels. Pharmacol Rev 57:473–508. doi:10.1124/pr.57.4.10

Heginbotham L, MacKinnon R (1993) Conduction properties of the cloned *Shaker* K^+ channel. Biophys J 65:2089–2096. doi:10.1016/S0006-3495(93)81244-X

Henrion U et al (2012) Tracking a complete voltage-sensor cycle with metal-ion bridges. Proc Natl Acad Sci USA 109:8552–8557. doi:10.1073/pnas.1116938109

Hess B, Bekker H, Berendsen HJ, Fraaije JG (1997) LINCS: a linear constraint solver for molecular simulations. J Comput Chem 18:1463–1472. doi:10.1002/(SICI)1096-987X(199709)18:12<1463:AID-JCC4>3.0.CO;2-H

Hess B, Kutzner C, Van Der Spoel D, Lindahl E (2008) GROMACS 4: algorithms for highly efficient, load-balanced, and scalable molecular simulation. J Chem Theory Comput 4:435–447. doi:10.1021/ct700301q

Hille B (1992) Ionic channels of excitable membranes. Sinauer, Sunderland

Hille B (2001) Ion channels of excitable membranes. Sinauer Associates, Sunderland

Hodgkin AL, Huxley AF (1990) A quantitative description of membrane current and its application to conduction and excitation in nerve. Bull Math Biol 52:25–71. doi:10.1007/BF02459568

Humphrey W, Dalke A, Schulten K (1996) VMD: visual molecular dynamics. J Mol Graph 14:33–38. doi:10.1016/0263-7855(96)00018-5

Jensen MØ et al (2010) Principles of conduction and hydrophobic gating in K^+ channels. Proc Natl Acad Sci USA 107:5833–5838. doi:10.1073/pnas.0911691107

Jensen MØ, Jogini V, Borhani DW, Leffler AE, Dror RO, Shaw DE (2012) Mechanism of voltage gating in potassium channels. Science 336:229–233. doi:10.1126/science.1216533

Jiang Y, Ruta V, Chen J, Lee A, MacKinnon R (2003) The principle of gating charge movement in a voltage-dependent K^+ channel. Nature 423:42–48. doi:10.1038/nature01581

Jogini V, Roux B (2007) Dynamics of the Kv1.2 voltage-gated K^+ channel in a membrane environment. Biophys J 93:3070–3082. doi:10.1529/biophysj.107.112540

Johnson M, Zaretskaya I, Raytselis Y, Merezhuk Y, McGinnis S, Madden TL (2008) NCBI BLAST: a better web interface. Nucleic Acids Res 36:W5–W9. doi:10.1093/nar/gkn201

Kabsch W, Sander C (1983) Dictionary of protein secondary structure: pattern recognition of hydrogen-bonded and geometrical features. Biopolymers 22:2577–2637. doi:10.1002/bip.360221211

Khalili-Araghi F, Jogini V, Yarov-Yarovoy V, Tajkhorshid E, Roux B, Schulten K (2010) Calculation of the gating charge for the Kv1.2 voltage-activated potassium channel. Biophys J 98:2189–2198. doi:10.1016/j.bpj.2010.02.056

Larkin MA et al (2007) Clustal W and Clustal X version 2.0. Bioinformatics 23:2947–2948. doi:10.1093/bioinformatics/btm404

Lee SY, Banerjee A, MacKinnon R (2009) Two separate interfaces between the voltage sensor and pore are required for the function of voltage-dependent K^+ channels. PLoS Biol 7:e47. doi:10.1371/journal.pbio.1000047

Long SB, Campbell EB, Mackinnon R (2005) Crystal structure of a mammalian voltage-dependent *Shaker* family K^+ channel. Science 309:897–903. doi:10.1126/science.1116269

Long SB, Tao X, Campbell EB, MacKinnon R (2007) Atomic structure of a voltage-dependent K^+ channel in a lipid membrane-like environment. Nature 450:376–382. doi:10.1038/nature06265

Mert T (2006) Kv1 channels in signal conduction of myelinated nerve fibers. Rev Neurosci 17:369–374. doi:10.1515/REVNEURO.2006.17.3.369

Milescu M, Bosmans F, Lee S, Alabi AA, Kim JI, Swartz KJ (2009) Interactions between lipids and voltage sensor paddles detected with tarantula toxins. Nat Struct Mol Biol 16:1080–1085. doi:10.1038/nsmb.1679

Nosé S (1984) A molecular dynamics method for simulations in the canonical ensemble. Mol Phy 52:255–268. doi:10.1080/00268978400101201

Papazian DM, Shao XM, Seoh SA, Mock AF, Huang Y, Wainstock DH (1995) Electrostatic interactions of S4 voltage sensor in *Shaker* K^+ channel. Neuron 14:1293–1301. doi:10.1016/0896-6273(95)90276-7

Parrinello M, Rahman A (1981) Polymorphic transitions in single crystals: a new molecular dynamics method. J Appl Phys 52:7182–7190. doi:10.1063/1.328693

Pathak MM et al (2007) Closing in on the resting state of the *Shaker* K^+ channel. Neuron 56:124–140. doi:10.1016/j.neuron.2007.09.023

Ruta V, Chen J, MacKinnon R (2005) Calibrated measurement of gating-charge arginine displacement in the KvAP voltage-dependent K^+ channel. Cell 123:463–475. doi:10.1016/j.cell.2005.08.041

Seoh SA, Sigg D, Papazian DM, Bezanilla F (1996) Voltage-sensing residues in the S2 and S4 segments of the *Shaker* K^+ channel. Neuron 16:1159–1167. doi:10.1016/S0896-6273(00)80142-7

Shealy RT, Murphy AD, Ramarathnam R, Jakobsson E, Subramaniam S (2003) Sequence-function analysis of the K^+-selective family of ion channels using a comprehensive alignment and the KcsA channel structure. Biophys J 84:2929–2942. doi:10.1016/S0006-3495(03)70020-4

Sigworth FJ (1994) Voltage gating of ion channels. Q Rev Biophys 27:1–40. doi:10.1017/S0033583500002894

Smith-Maxwell CJ, Ledwell JL, Aldrich RW (1998) Role of the S4 in cooperativity of voltage-dependent potassium channel activation. J Gen Physiol 111:399–420. doi:10.1085/jgp.111.3.399

Soler-Llavina GJ, Chang TH, Swartz KJ (2006) Functional interactions at the interface between voltage-sensing and pore domains in the *Shaker* K_v channel. Neuron 52:623–634. doi:10.1016/j.neuron.2006.10.005

Starace DM, Bezanilla F (2001) Histidine scanning mutagenesis of basic residues of the S4 segment of the *shaker* K^+ channel. J Gen Physiol 117:469–490. doi:10.1085/jgp.117.5.469

Swartz KJ (2004) Towards a structural view of gating in potassium channels. Nat Rev Neurosci 5:905–916. doi:10.1038/nrn1559

Swartz KJ (2008) Sensing voltage across lipid membranes. Nature 456:891–897. doi:10.1038/nature07620

Tao X, Lee A, Limapichat W, Dougherty DA, MacKinnon R (2010) A gating charge transfer center in voltage sensors. Science 328:67–73. doi:10.1126/science.1185954

Tiwari-Woodruff SK, Schulteis CT, Mock AF, Papazian DM (1997) Electrostatic interactions between transmembrane segments mediate folding of *Shaker* K^+ channel subunits. Biophys J 72:1489–1500. doi:10.1016/S0006-3495(97)78797-6

Tiwari-Woodruff SK, Lin MA, Schulteis CT, Papazian DM (2000) Voltage-dependent structural interactions in the *Shaker* K^+ channel. J Gen Physiol 115:123–138. doi:10.1085/jgp.115.2.123

Tombola F, Pathak MM, Isacoff EY (2005) Voltage-sensing arginines in a potassium channel permeate and occlude cation-selective pores. Neuron 45:379–388. doi:10.1016/j.neuron.2004.12.047

Tombola F, Pathak MM, Gorostiza P, Isacoff EY (2007) The twisted ion-permeation pathway of a resting voltage-sensing domain. Nature 445:546–549. doi:10.1038/nature05396

Treptow W, Tarek M (2006) Environment of the gating charges in the Kv1.2 *Shaker* potassium channel. Biophys J 90:L64–L66. doi:10.1529/biophysj.106.080754

Tu LW, Deutsch C (2010) A folding zone in the ribosomal exit tunnel for Kv1.3 helix formation. J Mol Biol 396:1346–1360. doi:10.1016/j.jmb.2009.12.059

Tusnady GE, Dosztanyi Z, Simon I (2005) TMDET: web server for detecting transmembrane regions of proteins by using their 3D coordinates. Bioinformatics 21:1276–1277. doi:10.1093/bioinformatics/bti121

Villalba-Galea CA, Sandtner W, Starace DM, Bezanilla F (2008) S4-based voltage sensors have three major conformations. Proc Natl Acad Sci USA 105:17600–17607. doi:10.1073/pnas.0807387105

Zagotta WN, Hoshi T, Aldrich RW (1994) *Shaker* potassium channel gating. III: evaluation of kinetic models for activation. J Gen Physiol 103:321–362. doi:10.1085/jgp.103.2.321

Zhou Y, MacKinnon R (2003) The occupancy of ions in the K^+ selectivity filter: charge balance and coupling of ion binding to a protein conformational change underlie high conduction rates. J Mol Biol 333:965–975. doi:10.1016/j.jmb.2003.09.022

Zhou M, MacKinnon R (2004) A mutant KcsA K^+ channel with altered conduction properties and selectivity filter ion distribution. J Mol Biol 338:839–846. doi:10.1016/j.jmb.2004.03.020

Zhu J et al (2003) Allowed N-glycosylation sites on the Kv1.2 potassium channel S1-S2 linker: implications for linker secondary structure and the glycosylation effect on channel function. Biochem J 375:769–775. doi:10.1042/BJ20030517

Zuberi SM et al (1999) A novel mutation in the human voltage-gated potassium channel gene (Kv1.1) associates with episodic ataxia type 1 and sometimes with partial epilepsy. Brain 122(Pt 5):817–825. doi:10.1093/brain/122.5.817